Electrophysiological Simulation of Maternal-Fetal ECG on a 3D Maternal Torso Model

Julie J Uv, Hermenegild Arevalo

Simula Research Laboratory, Oslo, Norway

Abstract

Congenital heart disease (CHD) is a leading cause of infant death. To diagnose CHD, recordings from abdominal fetal electrocardiograms (fECG) can be used as a non-invasive tool. However, it is challenging to extract the fetal signal from fECG recordings partly due to the lack of data combining fECG recordings with a ground truth for the fetal signal, which can be obtained by using a scalp electrode during delivery. In this study, we present a computational model of a pregnant female torso, in which we simulate fetal and maternal ventricular excitation during sinus rhythm to derive fECGs, so as to enable isolated measurement of the fetal and maternal signal contributions.

1. Introduction

Congenital heart disease (CHD) is a common birth defect arising in early pregnancy stages during the development of the heart [1], and is a leading cause of infant death with a prevalence of about 7–10 per 1000 live births [2,3]. Diagnosing CHD during pregnancy has been found to decrease risk of mortality and improve patient outcome following post natal surgery [4]. The current most common fetal monitoring technique is Doppler ultrasound, used in for instance cardiotocography (CTG). However, the waveform of the electrocardiogram (ECG) may contain important information about the cardiac electric activity beyond what CTG provides [5].

Currently, analysing the fetal ECG non-invasively is challenging mainly because of the low signal-to-noise ratio. A lack of limited reference data, comprising simultaneous non-invasive fetal ECG recordings from abdominal electrodes and an invasive fetal scalp electrode, further complicates the extraction of the direct fetal signal [6]. Previous work has addressed the lack of data by creating a fetal ECG simulator in which each cardiac source is represented by a moving dipole [7]. In this study, we simulate the fetal and maternal cardiac activity using an image-based finite element model to obtain realistic abdominal electrocardiogram.
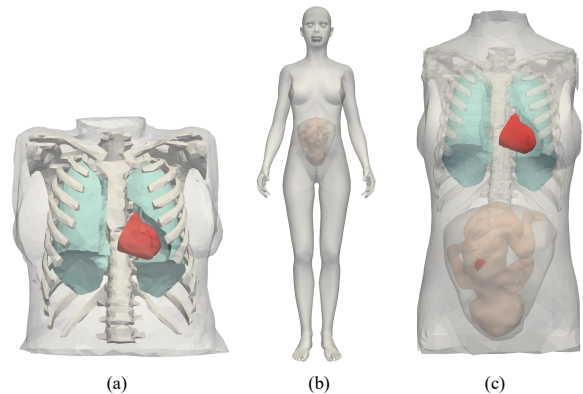

Figure 1. Combination of (a) Oxford and (b) Femonum model into the (c) pregnant torso model.

2. Materials & Methods

2.1. Geometrical mesh construction

A geometrical mesh was constructed by combining an MRI-based whole body pregnant model [8–10] with a cardiac biventricular geometry built from CT images embedded in an anatomical female torso [11]. The biventricular geometry was used to represent both the maternal and the fetal heart.

The combination of models was performed by scaling, translating and rotating the female torso to match the pregnant whole body model using Paraview [12], as well as adapting the biventricular geometry to the fetus (Figure 1).

Manual adjustments were to made the maternal ribcage and uterus in Meshmixer [13] to avoid overlapping mesh surfaces. A finite element volume mesh consisting of almost 18 million tetrahedral elements with an average element size of 500 μm was generated using `gmsh` [14]. The myocardial fiber orientations were assigned using a rule-based method [15]. To represent the vernix caseosa; a low-conducting layer which is present on the skin of the fetus during the last trimester [16], all elements directly connected to the nodes on the fetal body surface mesh were

Table 1. Conductivity values for extracardiac tissue.

Tissue	Conductivity (S m^{-1})	Reference
Amniotic fluid[1]	1.25	[22]
Torso and fetus	0.216	[21]
Maternal rib cage	0.02	[21]
Maternal lungs	$3.89 \cdot 10^{-2}$	[21]
Vernix caseosa	10^{-5}	[23]

[1] Value chosen to reflect third trimester (week 27-40).

classified as vernix caseosa.

2.2. Electrophysiological properties

2.2.1. Ionic models and assigned conductivities

Ionic current properties of the maternal heart were modelled using the Ten Tusscher model of human ventricular cardiomyocytes [17] . For the fetal heart, a modified version of [17] adapted to match fetal ventricular electrophysiology, was used [18]. Tissue propagation was modelled with the pseudo-bidomain approach [19] as implemented in openCARP [20] with a time step of 10 μs. Following [21], intracellular and extracellular conductivity tensors in the myocardium were set to $g_i = (0.27, 0.081, 0.045)$ and $g_e = (0.9828, 0.3654, 0.3654)$ S m^{-1} in the longitudinal, transverse and normal direction. For the extracardiac tissue, the assigned isotropic conductivities can be found in table 1.

In accordance with [21], the epi-, mid-myo and endocardial layers were defined as 30, 25 and 45 % of the myocardial width. In addition, the delayed rectifier current (IKs) was adjusted with an exponential gradient scaling between the apex and base, with 5.0 and 0.2 as the respective boundary values.

2.3. Stimulation protocol

Sinus rhythm was simulated over 2.5 seconds by pacing both hearts. Maternal stimuli were delivered in a ordered manner to 6 activation sites at 4 time intervals to reproduce results consistent with experimental findings as found in [24] with a strength of 100 μA/cm^2. Fetal stimuli were delivered to all endocardial nodes simultanously with a strength of 25 μA/cm^2. Basic cycle lengths were set to 690 and 450 ms for the maternal and fetal heart respectively [25, 26].

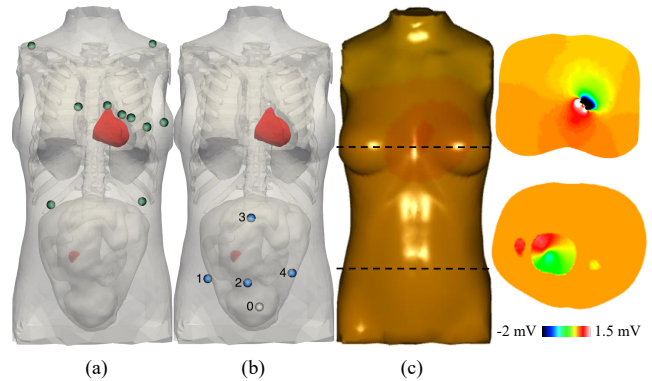(a)   (b)   (c)

-2 mV ▇▇▇ ▇▇ 1.5 mV

Figure 2. Electrode placement for (a) 12 lead ECG (b) maternal abdominal channels (numbered 1-4) and reference electrode (numbered 0). (c) Extracellular potential at $t = 31$ ms.

2.3.1. ECG measurements

In addition to the standard 12 lead ECG, the body surface potential was extracted at 4 abdominal electrodes and one reference electrode in order to replicate clinical measurements [27] [28]. The electrode set up can be seen in Figure 2. The ECG traces were calculated as the potential difference between the abdominal electrodes and the reference electrode located on the mid lower abdomen. The fetal signal was calculated in correspondence with the fetal scalp ECG, i.e. as the potential difference at the fetal scalp and an electrode corresponding to the maternal thigh.

3. Results

The extracellular potential shortly after first activation can be seen in Figure 2c for the torso as well as two cross sections at the maternal and fetal heart. The 12 lead ECG for the mother was computed and can be seen in figure 3 which matches well with a clinical ECG recording of a 35 year old female (dashed line) [28, 29].

The 4 abdominal channels can be seen in figure 4 and the fetal scalp ECG in figure 5. The recordings are compared to simultaneous recordings of abdominal and fetal scalp electrode during labour [27] [28]. In order to easier compare synthetic and clinical signals, the abdominal and fetal scalp ECGs have been scaled between 0 and 1.

Estimated ECG features are calculated for both maternal and fetal cardiac activity and compared to reference values in table 2 and 3 respectively.
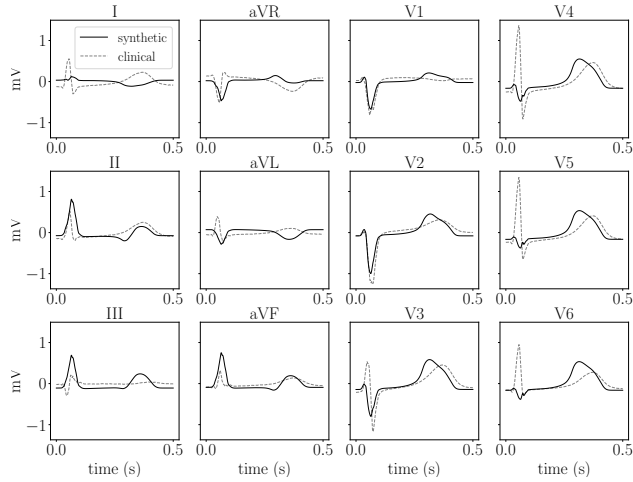
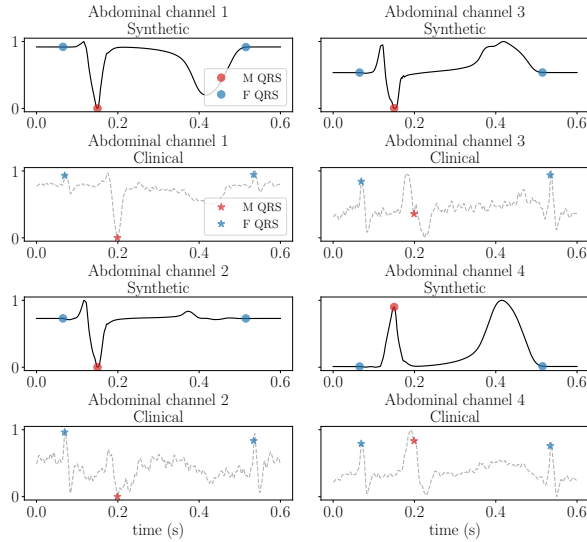Figure 3. Twelve lead ECG of synthetic and clinical recordings.

Figure 4. Four maternal abdominal electrodes of synthetic and clinical recordings. Synthetic and clinical maternal and fetal QRS complexes are marked with red and blue circles and stars respectively.
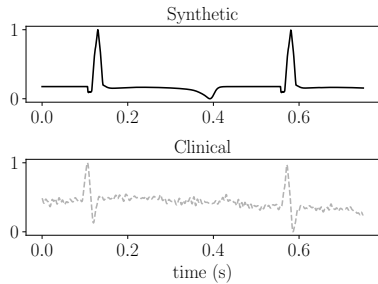

Figure 5. Fetal scalp electrode from simulation compared to clinical fetal scalp electrode recording.

Table 2. Calculated ECG features of maternal signal.

Feature	Unit	Value	Reference values
QTd	ms	430.00 ± 4.97	390, 460 [30]
QTc[2]	ms$^{1/2}$	517.66 ± 5.98	370, 480 [31]
RR	ms	690	655, 795 [25]

[2] Bazett´s formula.

Table 3. Calculated ECG features of fetal signal.

Feature	Unit	Value	Reference values
QTd	ms	276.75 ± 13.27	232, 295 [26] [3]
QTc	ms$^{1/2}$	412.55 ± 19.79	352.9, 448.1 [26] [3]
RR	ms	450	370, 470 [26] [4]

[3] Values chosen for week 29-35. [4] Approximate values at week 27-28.

4. Discussion

We can observe some differences between the simulated and clinical maternal 12 lead ECG, particularly for QRS complexes in lead V5 and V6. However, the close match in the morphologies is quite good considering we did not do personalization of the electrophysiological parameters. The deviation from the clinical recordings could be due to electrode placement.

For the abdominal ECG, we can see a similar shape in terms of direction of QRS complex and maternal T-wave. For the synthetic signal, we can observe a more prominent maternal T-wave, and a smaller fetal R-peak amplitude due to the low conducting vernix caseosa layer.

Comparing the fetal scalp ECG, we can observe a more prominent fetal T-wave for the synthetic signal, as well as a larger fetal R-peak amplitude.

Furthermore, the fetal and maternal QT duration and fetal corrected QT duration were consistent with clinical observations. The maternal corrected QT duration is higher than defined physiological normal ranges. However, the maternal basic cycle length at 690 ms is slightly shorter than normal non-pregnant basic cycle length, and Bazett´s formula has been found to overcorrect for higher heart rates [32].

5. Conclusion

We successfully created an anatomically detailed and biophysically accurate pregnant torso model that can simulate realistic body surface recordings. Simulations using this model may enable improvements in the recording and processing capabilities for fECGs, the reliable estimation of fetal heart rates, and possibly interpretation of fetal signal morphologies that could improve the overall diagnos-

tic significance of abdominal fECGs. In future work, we plan to further investigate the effects of the vernix caseosa layer in dampening the fetal heart signal. Additionally, the model generation pipeline developed in this study allows for the generation of other realistic pregnant torso models that can represent different fetal stages of development.

References

[1] Sameni R, Clifford GD. A review of fetal ECG signal processing; issues and promising directions. Open Pacing Electrophysiol Ther J 2010;3:4.

[2] Bruneau BG. The developmental genetics of congenital heart disease. Nature 2008;451(7181):943–948.

[3] Nembhard WN, Pathak EB, Schocken DD. Racial/ethnic disparities in mortality related to congenital heart defects among children and adults in the United States. Ethn Dis 2008;18(4):442–449.

[4] Nisselrooij AELV, et al. Why are congenital heart defects being missed? UOG 2020;55(6):747–757.

[5] Durosier DL, et al. Sampling rate of heart rate variability impacts the ability to detect acidemia in ovine fetuses near-term. Front Pediatr 2014;2:38.

[6] Matonia A, et al. Fetal electrocardiograms, direct and abdominal with reference heartbeat annotations. Sci Data 2020;7(1):200.

[7] Behar J, et al. An ECG simulator for generating maternal-foetal activity mixtures on abdominal ECG recordings. Physiol Meas 2014;35(8):1537.

[8] Bibin L, et al. Whole-body pregnant woman modeling by digital geometry processing with detailed uterofetal unit based on medical images. IEEE Trans Biomed 2010; 57(10):2346–2358.

[9] Dahdouh S, et al. A comprehensive tool for image-based generation of fetus and pregnant women mesh models for numerical dosimetry studies. Phys Med Biol 2014; 59(16):4583.

[10] Daz3D Studio, 2000. www.daz3d.com.

[11] Martinez-Navarro H, Rodriguez B, Bueno-Orovio A, Minchole A. Repository for modelling acute myocardial ischemia: simulation scripts and torso-heart mesh 2019;.

[12] Ayachit U. The paraview guide: a parallel visualization application. Kitware, Inc., 2015.

[13] Meshmixer. https://www.meshmixer.com.

[14] Geuzaine C, Remacle JF. Gmsh: A 3-D finite element mesh generator with built-in pre- and post-processing facilities. IJNME 2009;79(11):1309–1331.

[15] Streeter JDD, et al. Fiber orientation in the canine left ventricle during diastole and systole. Circ Res 1969;24(3):339–347.

[16] Oostendorp TF, van Oosterom A, Jongsma HW. Electrical properties of tissues involved in the conduction of foetal ECG. Med Biol Eng Comput 1989;27(3):322-–324.

[17] Tusscher KHT, Panfilov AV. Alternans and spiral breakup in a human ventricular tissue model. Am J Physiol Heart Circ Physio 2006;291(3):H1088–H1100.

[18] Pervolaraki E, Hodgson S, Holden AV, Benson AP. Towards computational modelling of the human foetal electrocardiogram: normal sinus rhythm and congenital heart block. Europace 2014;16(5):758–765.

[19] Bishop MJ, Plank G. Bidomain ECG simulations using an augmented monodomain model for the cardiac source. IEEE Trans Biomed Eng 2011;58(8):2297–2307.

[20] Plank G, et al. The openCARP simulation environment for cardiac electrophysiology. Comput Methods Programs Biomed 2021;208:106223.

[21] Martinez-Navarro H, et al. High arrhythmic risk in anteroseptal acute myocardial ischemia is explained by increased transmural reentry occurrence. Sci Rep 2019;9(1):1–12.

[22] Pachi A, et al. Use of electrical conductivity of amniotic fluid in the evaluation of fetal lung maturation. Fetal Diagn Ther 2001;16(2):90–94.

[23] Stinstra JG, Peters MJ. The influence of fetoabdominal tissues on fetal ECGs and MCGs. Arch Physiol Biochem 2002;110(3):165–176.

[24] Durrer D, et al. Total excitation of the isolated human heart. Circulation 1970;41(6):899–912.

[25] Loerup L, et al. Trends of blood pressure and heart rate in normal pregnancies: a systematic review and meta-analysis. BMC Med 2019;17(1):1–12.

[26] Strand SA, et al. Fetal magnetocardiogram waveform characteristics. Physiol Meas 2019;40(3):035002.

[27] Jezewski J, et al. Determination of fetal heart rate from abdominal signals: evaluation of beat-to-beat accuracy in relation to the direct fetal electrocardiogram. BMT 2012; 57(5):383–394.

[28] Goldberger AL, et al. PhysioBank, PhysioToolkit, and PhysioNet: components of a new research resource for complex physiologic signals. Circulation 2000;101(23):e215–e220.

[29] Bousseljot R, Kreiseler D, Schnabel A. Nutzung der EKG-Signaldatenbank CARDIODAT der PTB über das Internet 1995;317–318.

[30] Rautaharju AHA. ACCF/HRS Recommendations for the Standardization and Interpretation of the Electrocardiogram: Part iv: The ST segment, T and U waves, and the QT interval: A scientific statement from the American Heart Association Electrocardiography and Arrhythmias Committee, Council on Clinical Cardiology; the American College of Cardiology Foundation; and the Heart Rhythm Society: Endorsed by the International Society for Computerized Electrocardiology. Circulation ;(119):e241.

[31] Moss AJ. Measurement of the QT interval and the risk associated with QTc interval prolongation: a review. Am J Cardiol 1993;72(6):B23–B25.

[32] Davey P. How to correct the qt interval for the effects of heart rate in clinical studies. J Pharmacol Toxicol Methods 2002;48(1):3–9.

Address for correspondence:

Julie Johanne Uv
Kristian Augusts gate 23, 0164 Oslo, Norway
julie@simula.no